Title: Dynamin-2 facilitates Atg9 recycling from nascent autophagosomes

Authors: Alejandro Martorell Riera[1], Cinta Iriondo Martinez[1], Samuel Itskanov[1], Janos Steffen[2], Brett Roach[1], Carla M. Koehler[2] and Alexander M. van der Bliek[1]

Author affiliations: [1]Department of Biological Chemistry, David Geffen School of medicine at UCLA, [2]Department of Chemistry and Biochemistry, UCLA.

Send correspondence to: avan@mednet.ucla.edu

Autophagy involves rapid growth of phagophores through membrane addition. Newly added membranes are derived from other organelles through the formation of vesicles carrying the Atg9 protein. Membrane is delivered by fusing these vesicles with the phagophores. Atg9 is, nevertheless, not incorporated in autophagosomes. We now show that this protein is retrieved from phagophores by fission utilizing Dynamin-2 (Dnm2) as the membrane scission protein. Blocking Atg9 recycling by interfering with Dnm2 helps retain Atg9 in autophagosomes and degrades this protein by autophagy. Dnm2 colocalizes with the BAR domain protein Endophilin-B1 (EndoB1/Bif-1) when autophagy is induced, suggestive of transient interactions, but mutations in these proteins have very different effects from which we conclude that they act at different stages of autophagy. Our results show that Dnm2 promotes Atg9 retrieval, while EndoB1 may anchor the autophagy machinery. These data provide novel insights into the roles of membrane scission proteins during autophagy.

Introduction

Autophagy is a ubiquitous process for disposal of damaged cytoplasmic components and recycling of proteins during starvation (Choi, Ryter, and Levine 2013). Much has been learned about this process by studying a series of protein complexes that perform the rapid and intricate dance to form autophagosomes, which then fuse with lysosomes for degradation (Levine and Klionsky 2017). Autophagosomes are double membrane enclosures that fully seal off cargo destined for degradation in lysosomes (Bento et al. 2016). The membranes forming autophagosomes are derived from a variety of sources, including the plasma membrane, endosomes and the Golgi apparatus (Tooze 2013). These membranes are transported to nascent autophagosomes as vesicles carrying the Atg9 protein (Yamamoto et al. 2012). Atg9 is one of the few dedicated autophagy proteins with transmembrane segments. It was therefore surprising to find that Atg9 itself is not incorporated in autophagosomes (Orsi et al. 2012). Instead, the Atg9 protein must be retrieved after Atg9 vesicles

deliver their membrane to nascent autophagosomes. The mechanisms for Atg9 retrieval are currently unknown.

In this study, we focused on possible roles of Dynamin-2 (Dnm2) in autophagy. Dnm2 is one of three classic dynamins in mammalian cells (Schmid and Frolov 2011; Antonny et al. 2016; Ferguson and De Camilli 2012). Dnm2 is ubiquitously expressed, promoting membrane scission in a variety of different endocytic processes, including the formation of clathrin- or caveolin-coated vesicles and FEME (Renard et al. 2015), while dynamin-1 and dynamin-3 are primarily expressed in neurons where they act at pre- and post-synaptic densities in endocytosis (Ferguson and De Camilli 2012). Over the years, a number of alternative functions for Dnm2 have been proposed. Dnm2 was proposed to help generate exocytic vesicles that bud from the TGN (Jones et al. 1998; Liu et al. 2008), it was proposed to help generate actin comets emanating from endocytic vesicles (Lee and De Camilli 2002; Orth et al. 2002), it was proposed to facilitate a late stage of cytokinesis (Thompson et al. 2002), it was proposed to help regenerate autolysosomes during lipid droplet breakdown in hepatocytes (Schulze et al. 2013), it was proposed to help form ATG9 containing vesicles from recycling endosomes during autophagy (Takahashi et al. 2016) and most recently it was proposed to act in tandem with Drp1 during a late stage of mitochondrial fission (Lee et al. 2016). Many of these proposed functions await further verification, but not the role of dynamin 2 in endocytosis, because this has been observed in a wide range of different contexts.

All three dynamins have very similar sequences. Each one has five distinct protein domains: an N-terminal GTPase domain, a middle domain, a pleckstrin homology (PH) domain, a GTPase effector domain (GED) and a proline rich domain (PRD) (Ferguson and De Camilli 2012). The middle domain and GED fold back on each other to form a stalk, while the PH domain interacts with membranes and the PRD binds to SH3 domains in a range of different adaptor proteins (Gao et al. 2010; Chappie et al. 2010; Faelber et al. 2011; Ford, Jenni, and Nunnari 2011). A large pool of dynamin proteins exists as homomeric tetramers in the cytosol, but a small fraction gathers in spots on the plasma membrane to promote membrane scission (Schmid and Frolov 2011). Multiple contacts between adjacent dynamin molecules in those spots allows for assembly into chains, which then form multimeric spirals that wrap around the necks of budding endocytic vesicles and constrict to sever the membrane while hydrolyzing GTP (Schmid and Frolov 2011).

One of the deciding factors for targeting dynamins to different membranes is the presence or absence of specific binding partners. Dynamins interact with $PI(4,5)P_2$ at the plasma membrane (Achiriloaie, Barylko, and Albanesi 1999) and with SH3 domain containing proteins, such as amphiphysin and endophilin A during endocytosis (Simpson et al. 1999). Besides SH3 domains, amphiphysin and endophilin A both also have BAR domains, which bind to membranes and induce curvature through their concave shapes (Daumke, Roux, and Haucke 2014; McMahon and Boucrot 2015). Cooperative binding interactions between dynamin and amphiphysin or endophilin A have

been shown to help tubulate membranes *in vitro* and promote membrane severing *in vivo* (Meinecke et al. 2013; Renard et al. 2015; Farsad et al. 2001). Amphiphysin or endophilin A both have closely-related isoforms, amphiphysin-2 (Bin-1) and endophilin B1 (EndoB1/Bif1), that may act on other membranes (Lee et al. 2002; Farsad et al. 2001).

EndoB1 resides on ER membranes where it contributes to autophagosome formation by interacting with UVRAG, which is part of autophagy protein complexes built around Vps34 and Beclin-1 (Hurley and Young 2017; Takahashi et al. 2007). While studying the roles of EndoB1 during autophagy, we observed colocalization with Dnm2. This prompted us to further investigate a possible role of Dnm2 during autophagy. Surprisingly, our studies with knockout cells showed that EndoB1 and Dnm2 have opposite effects on apoptosis and on autophagy, which suggested to us that these proteins have different functions on the ER. Here, we show that Dnm2 and EndoB1 affect different stages of autophagy: EndoB1 is required at an early stage of autophagosome formation, while Dnm2 helps retrieve Atg9 from nascent autophagosomes.

Results

Dnm2 and EndoB1 colocalize when autophagy is induced.

To test for Dnm2 and EndoB1 colocalization, we conducted immunofluorescence experiments with wildtype MEF cells treated with or without rapamycin to induce autophagy. These cells were permeabilized with digitonin to improve the signal from membrane bound proteins by washing out soluble cytosolic proteins. We observed a marked increase in Dnm2 and EndoB1 colocalization after rapamycin treatment (Fig. 1a), as also determined with Mander's correlation coefficient (Fig. 1b) and with scatter plots (Suppl. Fig. 1-1a,b). Similar results were obtained with Pearson's correlation coefficient (not shown). To further test these interactions, we also used live cell imaging of transfected proteins with fluorescent tags as shown in Fig. 1c and Suppl. Fig. 1c (quantified in Fig. 1d and Suppl. Fig. 1-1c,d). In each of these cases, rapamycin and CCCP dramatically increased the degree of colocalization between Dnm2 and EndoB1.

We further investigated colocalization of endogenous Dnm2 and EndoB1 proteins, using proximity ligation assay (PLA) because this method has a high signal to noise ratio, only giving a signal when the two proteins are within 40nm of each other. We first verified the specificity of PLA using MEF cells with homozygous deletions in chromosomal Dnm2 and EndoB1 genes, as well as MEF cells with deletions in both genes. Lack of Dnm2 and EndoB1 expression in these cell lines was confirmed with Western blots (Suppl. Fig. 1-2). PLA for Dnm2 and EndoB1 in these homozygous knockout cells did not yield spots (Suppl. Fig. 1-3a) from which we conclude that PLA with Dnm2 and EndoB1 antibodies is highly specific. We also did not observe PLA spots when we used antibodies for

Fis1, a mitochondrial outer membrane facing the cytosol, and Hsp60, a mitochondrial matrix protein, suggesting that the distance between cytosol and mitochondrial matrix is enough to preclude PLA spots (Suppl. Fig. 1-3b). In contrast, PLA with antibodies for the bona fide partners MFF and Drp1 (Otera et al. 2010) yielded numerous spots, confirming the efficacy of this technique (Suppl. Fig. 1-3b).

PLA was used to assess colocalization of Dnm2 and EndoB1 under a variety of autophagy and apoptosis inducing conditions. We observed dramatic increases in PLA spots with each of the autophagy inducing conditions (Fig. 1e,f) in agreement with the colocalization observed by immunofluorescence and with fluorescent tagged proteins. We also expected an increase in numbers of colocalization spots during apoptosis, because Dnm2 and EndoB1 have both been connected apoptosis, albeit in different ways. Cytosolic Dnm2 promotes apoptosis in a p53 dependent manner (Fish, Schmid, and Damke 2000), while EndoB1 binds to Bax during apoptosis (Cuddeback et al. 2001). To our surprise, however, there was a decrease in PLA spots after treatment with apoptosis inducing chemicals. These results suggest that Dnm2 and EndoB1 have distinct functions during apoptosis and autophagy. The increase in PLA spots observed with autophagy-inducing conditions was, nevertheless, consistent with the increased colocalization observed with immunofluorescence of endogenous proteins and colocalization of transfected proteins. We therefore conclude that Dnm2 and EndoB1 colocalization increases during autophagy and decreases during apoptosis.

Lack of Dnm2 and EndoB1 effects on mitochondrial fission.

We used our knockout cells to determine whether Dnm2 or EndoB1 are required for mitochondrial fission, because both proteins were proposed to affect mitochondrial morphology in different contexts (Lee et al. 2016; Karbowski, Jeong, and Youle 2004) and their interactions could conceivably prime them for a role in mitochondrial fission. We induced mitochondrial fission with two well-established fission inducing conditions (30 min with CCCP or with valinomycin) (Ishihara et al. 2003; Yamano et al. 2014). Mitochondrial morphologies were observed by staining fixed cells for Tom20 (a mitochondrial outer membrane protein) and hsp60 (a matrix protein). There were no observable differences in mitochondrial morphologies between untreated wildtype cells, Dnm2 -/-, EndoB1 -/- or double knockout cells, nor were there noticeable differences between these cell types when they were treated with fission-inducing chemicals, as is evident from staining with mitochondrial matrix and outer membrane markers (Fig. 2a). For comparison, we also tested for mitochondrial fission in Drp1 knockout MEF cells, generated in parallel with the Dnm2 and EndoB1 knockout cells (Suppl. Fig. 2-1a). These cells have highly connected mitochondria, even after treatment with CCCP, which clearly distinguishes them from Dnm2 and EndoB1 knockout cells (Fig. 2b). The fission-inducing treatments resulted in highly fragmented mitochondria in WT, Dnm2 -/-, EndoB1 -/- and DKO

cells, but not in Drp1 -/- cells (Fig. 2c). Live cell imaging of mutant and wildtype cell lines also did not show differences in mitochondrial morphologies before or after treatment with CCCP (Suppl. Fig. 2-2). We conclude that Dnm2 and EndoB1 are not required for stress-induced mitochondrial fission. There are also no obvious differences in mitochondrial morphologies in untreated cells.

Mitochondrial fission could still be due to a compensatory response in Dnm2 knockout cells, for example through increased expression of another dynamin isoform. To address this possibility, we tested mitochondrial fission in a previously published conditional cell line in which all three dynamin genes (Dnm1, - 2 and -3) can be knocked out. Triple knockout cells, generated by growing the cell line with tamoxifen, have deletions in all three dynamin genes (Park et al. 2013). We verified this for Dnm1 and Dnm2 with Western blots (Suppl. Fig. 2-1b). We did not observe an effect on mitochondrial morphology in untreated cells, nor did we observe impairment of mitochondrial fission when these cells were treated with CCCP or valinomycin (Fig. 2d,e). Although it is unclear why we were unable to reproduce the previously reported effects of Dnm2 on mitochondrial fission (Lee et al. 2016), there could still be differences in cell lines or differences in approaches. We used knockout cells, while the previous study used siRNA raising the possibility of differences in compensatory responses. It is, nevertheless, clear from our results that Dnm2 is not required for mitochondrial fission in MEFs.

Dnm2 and EndoB1 have opposite effects on apoptosis.

Our PLA results showed fewer interactions between Dnm2 and EndoB1 when apoptosis is induced even though both proteins were previously suggested to contribute to apoptosis and they bind to each other *in vitro* (Soulet, Schmid, and Damke 2006; Cuddeback et al. 2001; Farsad et al. 2001), To corroborate this unexpected result, we further tested the effects of Dnm2 and EndoB1 deletions on apoptosis with two apoptosis inducing chemicals (staurosporine and actinomycin D) and three different assays (Bax recruitment to mitochondria, cytochrome c release from mitochondria and the formation of pyknotic nuclei) (Fig. 3a-c). For each these conditions, Dnm2 -/- cells showed a delay in the onset of apoptosis, while EndoB1 -/- cells showed more rapid onset of apoptosis. Dnm2-EndoB1 double knockout cells had an intermediate phenotype, which was not significantly different from wildtype. We conclude that Dnm2 has proapoptotic effects, but is not absolutely required for apoptosis, while EndoB1 is anti-apoptotic. To preclude the possibility that effects in the Dnm2 -/- cells are compensated by altered expression of the other two dynamin isoforms, we also tested apoptosis in the dynamin triple knockout cells. We observed a reduction in apoptosis after inducing loss of dynamin isoforms with tamoxifen (Fig. 3d), similar to the results obtained with the Dnm2 -/- cells.

The Dnm2 results are in line with previously reported results from other labs. The results obtained with EndoB1 mutants were, however, unanticipated, because this protein was also thought to be pro-apoptotic. Moreover, mutations in Dnm2 did not completely mask the effects of mutations in EndoB1 and vice versa, suggesting that Dnm2 and EndoB1 act in different pathways or that there are

other redundancies in this pathway. Reduced interactions between Dnm2 and EndoB1 in the PLA experiments and the lack of stronger effects in the triple mutant cell line argue against further redundancies in a single pathway and in favor of actions in different pathways during apoptosis. We conclude that Dnm2 has pro-apoptotic effects, but is not absolutely required for apoptosis, while EndoB1 is anti-apoptotic, but also only has moderate effects in these cell lines.

Effects of Dnm2 and EndoB1 deletions on autophagy

Since Dnm2 and EndoB1 colocalize when autophagy is induced, we tested whether both proteins contribute to this process. We first tested the effects of Dnm2 and EndoB1 deletions on CCCP induced mitophagy. Western blot analysis showed that LC3 lipidation is increased by deletion of EndoB1 alone, but not by Dnm2 deletion nor is it increased in the Dnm2 EndoB1 double knockout cells (Suppl. Fig. 4-1). Bafilomycin did not further increase the amount of lipidated LC3 in EndoB1 mutant cells suggesting that autophagy is triggered but the process is blocked at a later stage by the EndoB1 mutations. Mitophagy, as monitored by a decrease in hsp60 levels, is similarly impaired in the EndoB1 mutant, but not in Dnm2 or Dnm2 EndoB1 double mutant cells (Fig. 4a). These effects are more clearly demonstrated with images showing mitochondria in cells treated with CCCP (Fig. 4b). We then tested the effects of Dnm2 and EndoB1 deletions on starvation induced macro-autophagy. Western blot analysis showed that LC3 lipidation is inhibited by deletion of EndoB1 alone, but not by Dnm2 deletion nor is it impaired in the Dnm2 EndoB1 double knockout cells (Fig. 4c). similar effects were observed with p62 turnover, which is blocked in EndoB1 deletion cells, but not in Dnm2 or Dnm2 EndoB1 double knockout cells (Fig. 4c). Our results suggest that EndoB1 is necessary for progression of autophagy while the stage of inhibition depends on the inducing conditions. In contrast, mutations in Dnm2 do not inhibit autophagy and they are even able to suppress the inhibitory effects of mutations in EndoB1.

SIM images of GFP-LC3 and DsRed mitochondria in cells treated with CCCP show that cup shaped phagophores surround mitochondria in Dnm2 and Dnm2 EndoB1 knockout cells (Fig. 4d). These phagophores are indistinguishable from wildtype. In contrast, there were no cup shaped phagophores in EndoB1 knockout cells. GFP-LC3 did form aggregates but those appeared to be separate from mitochondria. There are several possible explanations for the seemingly normal progression or perhaps even acceleration of autophagy in Dnm2 -/- and Dnm2-EndoB1 DKO cells. First, EndoB1 could act in sequence with Dnm2, if Dnm2 is an inhibitor of autophagy and EndoB1 inhibits Dnm2. Second, Dnm2 could inhibit a third protein that is redundant with EndoB1. At present, we do not know which of these explanations is correct, but our results do unexpectedly show that Dnm2 is not needed for autophagy. It is at best neutral, or it may even be an inhibitor of autophagy.

To track the dynamics of autophagy in Dnm2 mutant cells lines, we transfected them with RFP-GFP-LC3, which is visible as yellow spots in the cytosol and red spots when autophagosomes

fuse with lysosomes, because acidification quenches GFP. Our results show that Dnm2 knockout cells have even larger numbers of red fluorescence spots than wildtype cells after treatment with CCCP (Fig. 4e,f). Autophagosomes in Dnm2 knockout cells appeared to have progressed more rapidly towards fusion with lysosomes than autophagosomes in wildtype cells treated with CCCP (Fig. 4g). Similar results were obtained with cells labeled for RFP-LC3 and the lysosomal marker GFP-Lamp1 (Fig. 4h). A possible explanation for this apparent increase comes from western blots showing that Dnm2 -/- cells accumulate mitophagy adaptor optineurin, while CCCP-induced degradation of optineurin continues even in the presence of Bafilomycin (Suppl. Fig. 4-1). Optineurin accumulation and turnover in Dnm2 -/- cells may be indirect effects of impaired endocytosis, because that process is also affected by optineurin function (Tumbarello et al. 2012; Vaibhava et al. 2012). It is, nevertheless, clear that Dnm2 -/- cells have no delays in mitophagy.

Dnm2 colocalizes with autophagic membranes.

To understand why Dnm2 and EndoB1 colocalize during autophagy even though their interactions appear to be inhibitory, we first looked for colocalization of Dnm2-EndoB1 PLA spots with other proteins that are relevant for autophagy. We could easily observe colocalization of the PLA spots with EGFP-LC3 when autophagy was induced (Fig. 5a). The relative numbers of Dnm2-EndoB1 PLA spots increase with autophagy inducing treatments, while Dnm2-EndoA1 spots decrease suggesting a shift from endocytosis to autophagy (Fig. 5b). We then tested for colocalization of PLA spots with a number of other autophagy related proteins. Results, summarized in Fig 5c, show a dramatic increase in the fraction of Dnm2-EndoB1 PLA spots associated with LC3. There was also a modest increase in the fraction associated with UVRAG, consistent with interactions close to the origins of autophagic membranes. In contrast there was a decrease in the fractions of PLA spots associated with LAMP1, which may reflect a shift away from the previously observed role in autophagolysosomal recycling (Schulze et al. 2013), and no change in the small fraction of PLA spots associated with Rab11, suggesting that those spots might not be relevant for autophagy. We conclude that a large fraction Dnm2-EndoB1 PLA spots are indeed at or near the origins of autophagosome membranes.

We also observed strong colocalization of GFP-tagged Dnm2 with RFP-LC3 when those tagged proteins were expressed in Dnm2 knockout cells, but not in wildtype cells (Fig. 4d). Colocalizing spots disappeared when the transfected cells were treated with the PIKfyve inhibitor YM201636 (Fig. 4d). PIKfyve is a PIP kinase associated with endosomal traffic and autophagy, converting PI(3)P into PI(3,5)P_2, a PIP_2 variant that can activate dynamins *in vitro* (Yarar et al. 2008) and thus could conceivably promote Dnm2 assembly and activation during autophagy. We further tested for PIP_2 accumulates on autophagosomes in Dnm2 knockout cells using the PLC-delta PH domain fused to GFP as a marker for PIP_2. This marker also colocalizes with LC3 spots in Dnm2 cells

(Fig. 4e,f), suggesting that autophagy structures accumulate PIP_2 in Dnm2 knockout cells. We conclude that Dnm2 specifically localizes to nascent autophagosomes when autophagy is induced and that autophagosomes accumulate Dnm2 binding sites when Dnm2 is lacking.

Dnm2 is required for Atg9 retrieval from autophagosome.

We tested possible effects of Dnm2 on the retrieval of Atg9 from autophagic membranes, because this process may not be essential for further progression of autophagy but it would involve membrane scission. The Atg9 protein, which helps bring membrane to growing phagophores, is not normally incorporated in mature autophagosomes, suggesting that this protein is retrieved by a recycling mechanism. We first tested whether the block in retrieval could be detected with fluorescent proteins. Dnm2 and wildtype cells were transfected with RFP-tagged Atg9 and EGFP-LC3. We observed well-defined colocalization of Atg9 and LC3 in Dnm2 cells, but not in wildtype cells (Fig. 6a), as confirmed with Mander's coefficients (Fig. 6b). there was also a concomitant drop in the numbers of spots that were only labeled with Atg9, but not with LC3 (Fig 6c), consistent with the idea that fusion with phagophores depletes the supply of Atg9 vesicles. Similar changes in Atg9 colocalization with LC3 were observed with the dynamin inhibitor dynasore (Fig 6b,c) and with Dnm2 siRNA (Suppl. Fig. 6-1), which strengthens the conclusion that these effects are specific for dynamin.

We reasoned that SNARE proteins that are carried along with Atg9 vesicles could also be retrieved by a Dnm2-dependent process. We first tested colocalization of VAMP7, which is a v-SNARE on Atg9 vesicles (Yu, Chen, and Tooze 2017). Our results show increased colocalization with LC3 in Dnm2 -/- cells, and even more so after induction of mitophagy with CCCP (Fig. 6d,e). We could similarly detect increased colocalization of the Atg9 vesicle tether Fip200 with LC3 (Fig. 6f,g). Although this protein is not incorporated in autophagosomes and it is not membrane anchored, there could still be an increased association with LC3 due to the mistargeting of Atg9 protein to phagophores.

We then tested colocalization of Atg9 and Lamp1, which is a lysosomal protein that would normally not be near Atg9 vesicles. These cells were incubated with pepstatin and E64d to inhibit lysosomal degradation of Atg9. The results show dramatically increased colocalization of Atg9 with LAMP1 in Dnm2 -/- cells after induction with CCCP (Fig. 6h,i). Lastly, we used Western blots to determine Atg9 levels in Dnm2 -/- cells. These cells have lower levels of Atg9 protein than wild type cells (Fig. 6j). These levels further decrease when mitophagy is induced in Dnm2 knockout cells with CCCP. This additional decrease is halted with Bafilomycin, consistent with lysosomal targeting and degradation of Atg9 in Dnm2 -/- cells (Fig. 6j). These results show that Atg9 is consumed by autophagy in Dnm2 -/- cells but not in WT cells.

Together, these experiments show that Atg9 retrieval from autophagosomes is impaired in Dnm2 -/- cells. This process is likely separate from the pro-autophagic functions of EndoB1, because

Dnm2 and EndoB1 have very different effects on autophagy. We were also unable to co-immunoprecipitate Dnm2 and EndoB1, despite extensive trials with different inducing conditions, detergents and cross-linkers. These proteins are most likely in close proximity during the initiation of autophagy, but their functional differences suggest that they act separately. These results are summarized in a model showing the early actions of EndoB1 during the initiation of autophagy and the actions of Dnm2 at a later stage, which we now show promotes the recycling of Atg9 (Fig. 6k).

Discussion

Our data strongly support an unexpected role for Dnm2 during autophagy. It was previously shown that the Atg9 protein is carried with vesicles that fuse with phagophores, but this protein is absent from mature autophagosomes (Orsi et al. 2012). It was therefore suggested that Atg9 is recycled after Atg9 carrying vesicles deliver membrane to phagophores, but the mechanisms for recycling were unknown. We now provide five lines of evidence showing that Dnm2 is required for retrieval of Atg9 and other transmembrane proteins from phagophores.

First, we detected substantial colocalization of Atg9 with LC3 in Dnm2 -/- cells when autophagy is induced. These results suggest that transmembrane proteins in Atg9 vesicles mix with LC3 containing membranes when Dnm2 function is impaired. Similar effects were observed with other methods to impair Dnm2 function, such as Dnm2 siRNA and chemical inhibitors of Dnm2 function. Second, the numbers of Atg9 vesicles decreased when autophagy was induced in Dnm2 knockout cells, suggesting that Atg9 vesicles fail to reform after fusion with autophagosomes. Third, the levels of Atg9 protein were reduced in Dnm2 knockout cells and they were further reduced when autophagy was induced. This reduction is blocked by Bafilomycin, suggesting that Atg9 is incorporated in autophagosomes and degraded by autophagy when Dnm2 function is impaired. Fourth, SNARE proteins needed for fusion of Atg9 vesicles with autophagosomes were also mixed with LC3 when autophagy is induced in Dnm2 -/- cells. Fifth, Dnm2 colocalizes with EndoB1 and LC3 when autophagy is induced, as shown with a variety of different methods. Taken together, these data show that Dnm2 is required for recycling transmembrane proteins from nascent autophagosomes as shown in our model (Fig. 6k).

This new recycling function of Dnm2 is distinct from other functions previously proposed alongside its well-established roles in endocytosis. Dnm2 was proposed to play roles in severing vesicles from endosomes, promoting autophagolysosomal recycling and promoting mitochondrial fission in concert with Drp1. Our data do not support a role in mitochondrial fission, although we have not ruled out differences in experimental approaches, nor does it support a role in vesicle formation at endosomes during autophagy, since we could not detect increased association of Dnm2 and EndoB1

with Rab11. There was some association of Dnm2 and EndoB1 with Lamp1, suggesting that there could be a role for this pair of proteins in lysosomal recycling, as previously proposed for autophagolysosome recycling in hepatocytes (Schulze et al. 2013), but this association was not increased during autophagy. We therefore conclude that the autophagic functions of Dnm2 and EndoB1 are more restricted. Dnm2 specifically affects retrieval of Atg9 and other transmembrane proteins from nascent autophagosomes, while EndoB1 is needed to promote autophagy.

Distinct functions of Dnm2 and EndoB1 are supported by the effects of gene deletions on autophagy but also by their mirror image effects on apoptosis: Dnm2 deletions inhibit apoptosis, but not autophagy, while EndoB1 deletions accelerate apoptosis and inhibit autophagy. Additional support for distinct functions comes from the effects of double mutants. Dnm2 deletions fully suppress the inhibition of autophagy by EndoB1 deletions, suggesting that Dnm2 deletions uncover an alternative mechanism that replaces EndoB1 when Dnm2 and EndoB1 are both mutated. This alternative mechanism could be a protein that functionally replaces EndoB1 within the Vps34 complex, or it could be a redundant pathway, such as the formation of autophagosomes at alternative site (ERES versus MAM) (Hamasaki et al. 2013; Ge et al. 2013; Ge et al. 2017; Graef et al. 2013). In both cases, Dnm2 exerts an inhibitory effect that only becomes apparent when EndoB1 is mutated. The exact nature of this inhibitory effect will require further studies of changes in Dnm2 knockout cells.

The colocalization of Dnm2-GFP with RFP-LC3 in Dnm2 knockout cells suggest that autophagosomes have specific Dnm2 binding sites. These binding sites most likely include PIP_2, because a PIP_2 reporter (PLC-delta PH domain) also colocalizes with LC3. Moreover, colocalization of Dnm2-GFP and RFP-LC3 is reduced by the PIKfyve inhibitor YM201636. PIKfyve generates $PI(3,5)P_2$ from PI(3)P, which are all found on autophagic membranes (Martin et al. 2013). Dnm2 normally binds to $PI(4,5)P_2$ on the plasma membrane, but in vitro studies have shown dynamins can also bind to $PI(3,5)P_2$ (Yarar et al. 2008), raising the possibility that this lipid is the signal for Dnm2 localization to autophagic membranes. There are also a number of Dnm2 splice variants, some of which may have selective interactions at autophagosomes but those have yet to be identified as well (Cao, Garcia, and McNiven 1998; Liu et al. 2008).

Dnm2 mediates a range of membrane scission events at the plasma membrane. These include clathrin- and caveolin-dependent endocytosis (Henley et al. 1998; van der Bliek et al. 1993), fast endocytosis in concert with EndoA1 (Renard et al. 2015) and clathrin/caveolin-independent endocytosis (Conner and Schmid 2003). Kiss-and-run could, however, be a more relevant paradigm for Atg9 recycling at autophagosomes, because this mechanism is much simpler: it does not require additional vesicle budding proteins (Alabi and Tsien 2013). Lipids but not proteins could then be transferred through a transient fusion pore (Monck, Alvarez de Toledo, and Fernandez 1990). Dynamin-dependent kiss-and-run mechanisms were observed with secretory granule secretion and synaptic vesicle retrieval (Alabi and Tsien 2013). The only known components are the SNAREs for

vesicle fusion and dynamins for membrane scission (Holroyd et al. 2002). The SNAREs for homotypic fusion of Atg9 vesicles prior to fusion with the phagophore have been identified (VAMP7 is the vSNARE; Syntaxin 7, 8 and VTI1B are the t-SNAREs) (Yu, Chen, and Tooze 2017), but it is unclear whether these SNAREs also contribute to fusion with the phagophore. Future experiments will help determine which other proteins are involved and whether Atg9 retrieval indeed utilizes a kiss-and-run mechanism.

In conclusion, our results have helped define a novel function for Dnm2 during autophagy. The proposed role of Dnm2 as the membrane scission protein that promotes retrieval of Atg9 from autophagosomes is supported by gene deletions, inhibitors and colocalization studies. Lack of Dnm2 causes unintended autophagic degradation of Atg9 and it may upset the balance of other autophagic processes. We have also uncovered close proximity and genetic interactions with EndoB1 suggestive of as yet uncharacterized alternative mechanisms that may contribute to autophagy. Future studies should help clarify these additional roles for Dnm2 and EndoB1.

Materials and methods

Plasmids The pMito-DsRed2 plasmid was from Clontech. Addgene provided pcDNA3-mRuby2 (#40260), GFP-C1-PLCdelta-PH (#21179), WT Dyn2 pEGFP (#34686), Dyn2-pmCherryN1 (#27689), pMXs-puro GFP-UVRAG (#38267), ptfLC3 (#21074), ppMXs-puro-RFP-ATG9A (#60609), EGFP-LC3 (# 24920), pcDNA3-mRuby2 (#40260) and pmRFP-LC3 (#21073). F. X. Soriano (Department of Cell Biology, University of Barcelona) provided the GFP-Bax plasmid. E. C. Dell'Angelica (Department of Human Genetics, UCLA School of Medicine) provided the GFP-Lamp1 plasmid. To generate mRuby2-EndophilinB1, mRuby2 coding sequences from pcDNA3-mRuby2 were fused in frame to EndophilinB1 cDNA by PCR and inserted into pcDNA3 (Invitrogen).

Cell culture, transfection, gene knockout and chemical treatments. MEF cells were grown in DMEM with 10% FCS. Transient transfections were done with jetPRIME following manufacturer's instructions (Polyplus). For siRNA, cells were grown in 6cm dishes, transfected with 50nM oligonucleotides using RNAimax (Invitrogen) and analyzed 72h later. MEF cells with conditional knockout of all three dynamin isoforms (TKO) were obtained from P. De Camilli (Yale School of Medicine, New Haven). Growth and conditional knockout procedures for these cells were as described (Ferguson et al. 2009; Raimondi et al. 2011; Park et al. 2013). Deletions in Dnm2, EndoB1 and Drp1 genes were introduced in MEF cells using CRISPR/Cas9 methods, as described (Ran et al. 2013). Target sites were identified using the Boutros Lab Website (http://www.e-crisp.org/E-CRISP/designcrispr.html). Dnm2 gRNA was: 5'-GATGGCAAACACGTGCTTGT-3'. EndoB1 gRNAs were: 5'-GCAGGAACTGAGTTTGGCCC-3'; and 5'-GGATTTCAACGTGAAGAAGC-3'. Drp1 gRNA was: 5'-GCAGTGGGAAGAGCTCAGTGC-3'. The gRNAs were cloned in the px459 plasmid,

containing puromycin resistance and Cas9 genes, and 1.2μg was transfected into MEF cells, followed by 24hr puromycin selection. Surviving colonies were isolated, genotyped and analyzed with western blots.

Amino acid starvation was induced by washing cells twice in EBSS with calcium and magnesium (Thermo Fisher Scientific), and incubated for the indicated length of time. The following chemicals with their final concentrations were from Sigma-Aldrich: 20μM CCCP, 40μg/ml antimycin A, 10μM ionomycin, 10μM actinomycin D and 1μM 4-Hydroxy Tamoxifen. The following chemicals with their final concentrations were from InvivoGen: 0.5μM Bafilomycin A1, 10μM rapamycin and 1μM YM-201636. Staurosporine (Thermo Fisher Scientific) was used at 2μM. Z-VAD-FMK (BD Bioscience) was used at 20μM. Dynasore (EMD Millipore) was used at 80μM.

Immunoblotting, immunofluorescence, and proximity ligation assay. Total cell lysates for Western blots were made with RIPA buffer. Samples were subjected to SDS-PAGE, transferred to nitrocellulose or PVDF membranes, blocked with Odyssey Blocking Buffer (LI-COR), and incubated overnight at 4°C with primary antibodies. Membranes were then washed with PBS-T and incubated with IRDye 800CW or 670RD secondary antibodies (LI-COR). Fluorescent bands were detected with an Odyssey scanner and analyzed with Image Studio Software (LI-COR). For immunofluorescence, cells were grown on 12mm coverslips, fixed for 10min with 4% paraformaldehyde in PBS, and permeabilized for 5min with 0.1% Triton X-100 in PBS, blocked for 1h with Goat or Donkey Serum in PBS-T and incubated with primary antibodies. For immunofluorescence of Dnm2, cells were first permeabilized with 0.05% digitonin to wash out soluble cytosolic proteins. Secondary antibodies were Alexa Fluor 488-, 594- or 647-conjugated goat anti-mouse or rabbit IgG (Invitrogen). Proximity ligation assays were conducted with Duolink as recommended by the manufacturer (Sigma-Aldrich).

Antibodies Rabbit anti-Endophilin A1, mouse anti-SQSTM1 (p62), rabbit anti-dynamin 1, rabbit anti-dynamin 2, mouse anti-Hsp60, rabbit anti-cytochrome c and mouse anti-VDAC1/Porin were from Abcam. Rabbit anti-LC3B and mouse anti-tubulin antibodies were from Sigma Aldrich. Goat anti-dynamin 2 and rabbit anti-Tom20 were from Santa Cruz Biotechnology. Mouse anti-Tim23 and mouse anti-Drp1 were from BD Biosciences. Rabbit anti-OPTN was from Proteintech. Mouse anti-Endophilin B1 was from Imgenex.

Fluorescence microscopy. For live imaging, cells were grown in glass bottom dishes (MatTek). Cells were viewed with a Marianas spinning disc confocal from Intelligent Imaging, which uses an Axiovert microscope (Carl Zeiss Microscopy) with a CSU22 spinning disk (Yokogawa), an Evolve 512 EMCCD camera (Photometrics) and a temperature unit (Okolab). Cells were imaged at 37°C with 40x/1.4 and 100x/1.4 oil objectives. Super resolution images were acquired with SIM using a DeltaVision OMX SR (General Electric). Fiji ImageJ software was used for image analysis.

Acknowledgements

We are grateful for many helpful discussions and sharing of reagents with Lars Dreier, Yu (Sammy) Sun at UCLA. C.M.K. was supported by NIH grants R01GM61721, R01GM073981 and R01DK101780. A.M.v.d.B. was supported by HIH grant U01GM109764.

References

Achiriloaie, M., B. Barylko, and J. P. Albanesi. 1999. 'Essential role of the dynamin pleckstrin homology domain in receptor- mediated endocytosis', *Mol Cell Biol*, 19: 1410-5.

Alabi, A. A., and R. W. Tsien. 2013. 'Perspectives on kiss-and-run: role in exocytosis, endocytosis, and neurotransmission', *Annual review of physiology*, 75: 393-422.

Antonny, B., C. Burd, P. De Camilli, E. Chen, O. Daumke, K. Faelber, M. Ford, V. A. Frolov, A. Frost, J. E. Hinshaw, T. Kirchhausen, M. M. Kozlov, M. Lenz, H. H. Low, H. McMahon, C. Merrifield, T. D. Pollard, P. J. Robinson, A. Roux, and S. Schmid. 2016. 'Membrane fission by dynamin: what we know and what we need to know', *Embo J*, 35: 2270-84.

Bento, C. F., M. Renna, G. Ghislat, C. Puri, A. Ashkenazi, M. Vicinanza, F. M. Menzies, and D. C. Rubinsztein. 2016. 'Mammalian Autophagy: How Does It Work?', *Annu Rev Biochem*, 85: 685-713.

Cao, H., F. Garcia, and M. A. McNiven. 1998. 'Differential Distribution of Dynamin Isoforms in Mammalian Cells', *Mol Biol Cell*, 9: 2595-609.

Chappie, J. S., S. Acharya, M. Leonard, S. L. Schmid, and F. Dyda. 2010. 'G domain dimerization controls dynamin's assembly-stimulated GTPase activity', *Nature*, 465: 435-40.

Choi, A. M., S. W. Ryter, and B. Levine. 2013. 'Autophagy in human health and disease', *The New England journal of medicine*, 368: 1845-6.

Conner, S. D., and S. L. Schmid. 2003. 'Regulated portals of entry into the cell', *Nature*, 422: 37-44.

Cuddeback, S. M., H. Yamaguchi, K. Komatsu, T. Miyashita, M. Yamada, C. Wu, S. Singh, and H. G. Wang. 2001. 'Molecular cloning and characterization of Bif-1. A novel Src homology 3 domain-containing protein that associates with Bax', *J Biol Chem*, 276: 20559-65.

Daumke, O., A. Roux, and V. Haucke. 2014. 'BAR domain scaffolds in dynamin-mediated membrane fission', *Cell*, 156: 882-92.

Faelber, K., Y. Posor, S. Gao, M. Held, Y. Roske, D. Schulze, V. Haucke, F. Noe, and O. Daumke. 2011. 'Crystal structure of nucleotide-free dynamin', *Nature*, 477: 556-60.

Farsad, K., N. Ringstad, K. Takei, S. R. Floyd, K. Rose, and P. De Camilli. 2001. 'Generation of high curvature membranes mediated by direct endophilin bilayer interactions', *J Cell Biol*, 155: 193-200.

Ferguson, S. M., and P. De Camilli. 2012. 'Dynamin, a membrane-remodelling GTPase', *Nat Rev Mol Cell Biol*, 13: 75-88.

Ferguson, S. M., A. Raimondi, S. Paradise, H. Shen, K. Mesaki, A. Ferguson, O. Destaing, G. Ko, J. Takasaki, O. Cremona, O' Toole E, and P. De Camilli. 2009. 'Coordinated actions of actin and BAR proteins upstream of dynamin at endocytic clathrin-coated pits', *Dev Cell*, 17: 811-22.

Fish, K. N., S. L. Schmid, and H. Damke. 2000. 'Evidence that dynamin-2 functions as a signal-transducing GTPase', *J Cell Biol*, 150: 145-54.

Ford, M. G., S. Jenni, and J. Nunnari. 2011. 'The crystal structure of dynamin', *Nature*, 477: 561-6.

Gao, S., A. von der Malsburg, S. Paeschke, J. Behlke, O. Haller, G. Kochs, and O. Daumke. 2010. 'Structural basis of oligomerization in the stalk region of dynamin-like MxA', *Nature*, 465: 502-6.

Ge, L., D. Melville, M. Zhang, and R. Schekman. 2013. 'The ER-Golgi intermediate compartment is a key membrane source for the LC3 lipidation step of autophagosome biogenesis', *eLife*, 2: e00947.

Ge, L., M. Zhang, S. J. Kenny, D. Liu, M. Maeda, K. Saito, A. Mathur, K. Xu, and R. Schekman. 2017. 'Remodeling of ER-exit sites initiates a membrane supply pathway for autophagosome biogenesis', *EMBO Rep*, 18: 1586-603.

Graef, M., J. R. Friedman, C. Graham, M. Babu, and J. Nunnari. 2013. 'ER exit sites are physical and functional core autophagosome biogenesis components', *Mol Biol Cell*, 24: 2918-31.

Hamasaki, M., N. Furuta, A. Matsuda, A. Nezu, A. Yamamoto, N. Fujita, H. Oomori, T. Noda, T. Haraguchi, Y. Hiraoka, A. Amano, and T. Yoshimori. 2013. 'Autophagosomes form at ER-mitochondria contact sites', *Nature*, 495: 389-93.

Henley, J. R., E. W. Krueger, B. J. Oswald, and M. A. McNiven. 1998. 'Dynamin-mediated internalization of caveolae', *J Cell Biol*, 141: 85-99.

Holroyd, P., T. Lang, D. Wenzel, P. De Camilli, and R. Jahn. 2002. 'Imaging direct, dynamin-dependent recapture of fusing secretory granules on plasma membrane lawns from PC12 cells', *Proc Natl Acad Sci U S A*, 99: 16806-11.

Hurley, J. H., and L. N. Young. 2017. 'Mechanisms of Autophagy Initiation', *Annu Rev Biochem*, 86: 225-44.

Ishihara, N., A. Jofuku, Y. Eura, and K. Mihara. 2003. 'Regulation of mitochondrial morphology by membrane potential, and DRP1-dependent division and FZO1-dependent fusion reaction in mammalian cells', *Biochem Biophys Res Commun*, 301: 891-8.

Jones, S. M., K. E. Howell, J. R. Henley, H. Cao, and M. A. McNiven. 1998. 'Role of dynamin in the formation of transport vesicles from the trans- Golgi network', *Science*, 279: 573-7.

Karbowski, M., S. Y. Jeong, and R. J. Youle. 2004. 'Endophilin B1 is required for the maintenance of mitochondrial morphology', *J Cell Biol*, 166: 1027-39.

Lee, E., and P. De Camilli. 2002. 'Dynamin at actin tails', *Proc Natl Acad Sci U S A*, 99: 161-6.

Lee, E., M. Marcucci, L. Daniell, M. Pypaert, O. A. Weisz, G. C. Ochoa, K. Farsad, M. R. Wenk, and P. De Camilli. 2002. 'Amphiphysin 2 (Bin1) and T-tubule biogenesis in muscle', *Science*, 297: 1193-6.

Lee, J. E., L. M. Westrate, H. Wu, C. Page, and G. K. Voeltz. 2016. 'Multiple dynamin family members collaborate to drive mitochondrial division', *Nature*, 540: 139-43.

Levine, B., and D. J. Klionsky. 2017. 'Autophagy wins the 2016 Nobel Prize in Physiology or Medicine: Breakthroughs in baker's yeast fuel advances in biomedical research', *Proc Natl Acad Sci U S A*, 114: 201-05.

Liu, Y. W., M. C. Surka, T. Schroeter, V. Lukiyanchuk, and S. L. Schmid. 2008. 'Isoform and splice-variant specific functions of dynamin-2 revealed by analysis of conditional knock-out cells', *Mol Biol Cell*, 19: 5347-59.

Martin, S., C. B. Harper, L. M. May, E. J. Coulson, F. A. Meunier, and S. L. Osborne. 2013. 'Inhibition of PIKfyve by YM-201636 dysregulates autophagy and leads to apoptosis-independent neuronal cell death', *PLoS One*, 8: e60152.

McMahon, H. T., and E. Boucrot. 2015. 'Membrane curvature at a glance', *J Cell Sci*, 128: 1065-70.

Meinecke, M., E. Boucrot, G. Camdere, W. C. Hon, R. Mittal, and H. T. McMahon. 2013. 'Cooperative recruitment of dynamin and BIN/amphiphysin/Rvs (BAR) domain-containing proteins leads to GTP-dependent membrane scission', *J Biol Chem*, 288: 6651-61.

Monck, J.R., G. Alvarez de Toledo, and J.M. Fernandez. 1990. 'Tension in secretory granule membranes causes extensive membrane transfer through exocytotic fusion pore', *Proc. Natl. Acad. Sci. USA*, 87: 7804-08.

Orsi, A., M. Razi, H. C. Dooley, D. Robinson, A. E. Weston, L. M. Collinson, and S. A. Tooze. 2012. 'Dynamic and transient interactions of Atg9 with autophagosomes, but not membrane integration, are required for autophagy', *Mol Biol Cell*, 23: 1860-73.

Orth, J. D., E. W. Krueger, H. Cao, and M. A. McNiven. 2002. 'The large GTPase dynamin regulates actin comet formation and movement in living cells', *Proc Natl Acad Sci U S A*, 99: 167-72.

Otera, H., C. Wang, M. M. Cleland, K. Setoguchi, S. Yokota, R. J. Youle, and K. Mihara. 2010. 'Mff is an essential factor for mitochondrial recruitment of Drp1 during mitochondrial fission in mammalian cells', *The Journal of cell biology*, 191: 1141-58.

Park, R. J., H. Shen, L. Liu, X. Liu, S. M. Ferguson, and P. De Camilli. 2013. 'Dynamin triple knockout cells reveal off target effects of commonly used dynamin inhibitors', *J Cell Sci*, 126: 5305-12.

Raimondi, A., S. M. Ferguson, X. Lou, M. Armbruster, S. Paradise, S. Giovedi, M. Messa, N. Kono, J. Takasaki, V. Cappello, E. O'Toole, T. A. Ryan, and P. De Camilli. 2011. 'Overlapping role of dynamin isoforms in synaptic vesicle endocytosis', *Neuron*, 70: 1100-14.

Ran, F. A., P. D. Hsu, J. Wright, V. Agarwala, D. A. Scott, and F. Zhang. 2013. 'Genome engineering using the CRISPR-Cas9 system', *Nature protocols*, 8: 2281-308.

Renard, H. F., M. Simunovic, J. Lemiere, E. Boucrot, M. D. Garcia-Castillo, S. Arumugam, V. Chambon, C. Lamaze, C. Wunder, A. K. Kenworthy, A. A. Schmidt, H. T. McMahon, C. Sykes, P. Bassereau, and L. Johannes. 2015. 'Endophilin-A2 functions in membrane scission in clathrin-independent endocytosis', *Nature*, 517: 493-6.

Schmid, S. L., and V. A. Frolov. 2011. 'Dynamin: functional design of a membrane fission catalyst', *Annu Rev Cell Dev Biol*, 27: 79-105.

Schulze, R. J., S. G. Weller, B. Schroeder, E. W. Krueger, S. Chi, C. A. Casey, and M. A. McNiven. 2013. 'Lipid droplet breakdown requires dynamin 2 for vesiculation of autolysosomal tubules in hepatocytes', *J Cell Biol*, 203: 315-26.

Simpson, F., N. K. Hussain, B. Qualmann, R. B. Kelly, B. K. Kay, P. S. McPherson, and S. L. Schmid. 1999. 'SH3-domain-containing proteins function at distinct steps in clathrin-coated vesicle formation', *Nat Cell Biol*, 1: 119-24.

Soulet, F., S. L. Schmid, and H. Damke. 2006. 'Domain requirements for an endocytosis-independent, isoform-specific function of dynamin-2', *Exp Cell Res*, 312: 3539-45.

Takahashi, Y., D. Coppola, N. Matsushita, H. D. Cualing, M. Sun, Y. Sato, C. Liang, J. U. Jung, J. Q. Cheng, J. J. Mule, W. J. Pledger, and H. G. Wang. 2007. 'Bif-1 interacts with Beclin 1 through UVRAG and regulates autophagy and tumorigenesis', *Nat Cell Biol*, 9: 1142-51.

Takahashi, Y., N. Tsotakos, Y. Liu, M. M. Young, J. Serfass, Z. Tang, T. Abraham, and H. G. Wang. 2016. 'The Bif-1-Dynamin 2 membrane fission machinery regulates Atg9-containing vesicle generation at the Rab11-positive reservoirs', *Oncotarget*, 7: 20855-68.

Thompson, H. M., A. R. Skop, U. Euteneuer, B. J. Meyer, and M. A. McNiven. 2002. 'The large GTPase dynamin associates with the spindle midzone and is required for cytokinesis', *Curr Biol*, 12: 2111-7.

Tooze, S. A. 2013. 'Current views on the source of the autophagosome membrane', *Essays Biochem*, 55: 29-38.

Tumbarello, D. A., B. J. Waxse, S. D. Arden, N. A. Bright, J. Kendrick-Jones, and F. Buss. 2012. 'Autophagy receptors link myosin VI to autophagosomes to mediate Tom1-dependent autophagosome maturation and fusion with the lysosome', *Nat Cell Biol*, 14: 1024-35.

Vaibhava, V., A. Nagabhushana, M. L. Chalasani, C. Sudhakar, A. Kumari, and G. Swarup. 2012. 'Optineurin mediates a negative regulation of Rab8 by the GTPase-activating protein TBC1D17', *J Cell Sci*, 125: 5026-39.

van der Bliek, A. M., T. E. Redelmeier, H. Damke, E. J. Tisdale, E. M. Meyerowitz, and S. L. Schmid. 1993. 'Mutations in human dynamin block an intermediate stage in coated vesicle formation', *J Cell Biol*, 122: 553-63.

Yamamoto, H., S. Kakuta, T. M. Watanabe, A. Kitamura, T. Sekito, C. Kondo-Kakuta, R. Ichikawa, M. Kinjo, and Y. Ohsumi. 2012. 'Atg9 vesicles are an important membrane source during early steps of autophagosome formation', *J Cell Biol*, 198: 219-33.

Yamano, K., A. I. Fogel, C. Wang, A. M. van der Bliek, and R. J. Youle. 2014. 'Mitochondrial Rab GAPs govern autophagosome biogenesis during mitophagy', *eLife*, 3: e01612.

Yarar, D., M. C. Surka, M. C. Leonard, and S. L. Schmid. 2008. 'SNX9 activities are regulated by multiple phosphoinositides through both PX and BAR domains', *Traffic*, 9: 133-46.

Yu, L., Y. Chen, and S. A. Tooze. 2017. 'Autophagy pathway: cellular and molecular mechanisms', *Autophagy*: 0.

Figure legends

Fig. 1. Colocalization of Dnm2 and EndoB1. (a) Immunofluorescence of endogenous Dnm2 (green) and EndoB1 (red) is shown without or with 2 hr rapamycin. (b) Mander's coefficients for colocalization shown for untreated cells and after 2 or 4 hr with rapamycin or CCCP (50 cells were counted per experiment, SD for 3 independent experiments, unpaired Student's t-test). (c and d) similar experiments with transfected cells expressing GFP-tagged dnm2 and mRuby2-tagged EndoB1. (e) Colocalization of Dnm2 and EndoB1 tested with Proximity Ligation Assay (PLA) shown with or without 2 hr Antimycin A treatment. (f) Average numbers of PLA dots/cell shown for Dnm2 and EndoB1 colocalization in untreated cells, cells treated with staurosporine (STS) or actinomycin D to induce apoptosis, or with CCCP, Antimycin A, rapamycin, starvation and ionomycin to induce autophagy. Numbers of dots were counted in 50 cells/experiment (n=3, unpaired student's t-test). Scale bar is 10 μm for whole cells and 5 μm for enlarged portions.

Fig. 2. Effects of Dnm2 and EndoB1 mutations on mitochondrial fission. (a) Immunofluorescence of cells stained with antibodies for Tom20 (red) and Hsp60 (green) show no effects of Dnm2 or EndoB1 mutations on mitochondrial fission. The top row has images of untreated cells, the middle row has cells treated for 30 min with CCCP and the bottom row has cells treated for 30 min with valinomycin to induce mitochondrial fission. (b) Images of Drp1 -/- cells treated without or with CCCP. (c) Histogram showing that mutations in Dnm2 and EndoB1 do not prevent CCCP or valinomycin induced mitochondrial fission. (d) Images of cells before and after treatment with tamoxifen to induce knockout of all three dynamin genes. Cells were then treated with CCCP or valinomycin to induce mitochondrial fission. (e) Histogram showing that mutations in all three dynamin genes do not prevent CCCP or valinomycin induced mitochondrial fission. 50 cells/experiment, n=3, unpaired student's t-test. Scale bar is 10 μm.

Fig. 3. Effects of Dnm2 and EndoB1 mutations on apoptosis. (a) Bax translocation to mitochondria is delayed when apoptosis is induced in Dnm2 -/- cells, but not in EndoB1 -/- cells. (b and c) Similar effects were observed with cytochrome c release from mitochondria and with the appearance of pyknotic nuclei, which are two other indicators of apoptosis. (d) Bax translocation to mitochondria is delayed in cells lacking all three dynamins. Triple knockout cells (TKO) were generated by treating conditional cells (labeled as WT) with tamoxifen to induce Cre recombinase. 50 cells per experiment, n=3, unpaired Student's t-test.

Fig. 4. Effects of Dnm2 and EndoB1 mutations on autophagy. (a) Western blots showing the effects of CCCP on mitophagy in Dnm2 and EndoB1 -/- cells. Loss of Hsp60 and porin at 8hr in Dnm2 -/- but to a lesser extent in EndoB1 -/- cells shows differential effects on mitophagy. At 24 hr, all mitochondrial proteins are being degraded, but the 8 hr time point suggests that this process is accelerated in Dnm2 -/- cells and delayed in EndoB1 -/- cells. (b) similar effects are observed with immunofluorescence microscopy using Tom20 (red) and Hsp60 (green) antibodies. (c) Starvation induced autophagy is not affected by mutations in Dnm2 or EndoB1 as shown with p62 turnover. Optineurin accumulates in Dnm2 -/- cells, but is also degraded when autophagy is induced. (d) Super-resolution images (SIM) show the formation of LC3-membranes (green) encapsulating mitochondria (red) in cells treated with CCCP. These structures are observed in WT, Dnm2 -/- and DKO cells, but not in EndoB1 -/- cells. Cells were treated for 6 hr with 20 μM CCCP. Mitochondria were detected with mitoRFP and autophagic membranes were detected with EGFP-LC3. (e) Tracking autophagy with RFP-GFP-LC3 marker shows transfer of LC3 to autophagolysomes, visible as red spots due to acidic quenching of GFP. (f) Numbers of autophagosomes per cells, detected as yellow spots are increased in Dnm2 -/- cells. (g) numbers of autophagolysosomes, detected as red spots, are dramatically increased in Dnm2 -/- cells treated with CCCP. (h) Colocalization of LC3 with Lamp1 is similarly increased in Dnm2 -/- cells. For the histograms, 50 cells per experiment, n=3, unpaired Student's t-test. Scale bar is 10 μm, except in the bottom row of panel d, where the bar is 1 μm.

Fig. 5. Colocalization of Dnm2 with autophagy proteins. (a) Despite different effects of Dnm2 and EndoB1 on autophagy, PLA spots for endogenous Dnm2 and EndoB1 (red) do colocalize with EGFP-LC3 (green), when autophagy is induced (4 hr CCCP). (b) Relative numbers Dnm2-EndoB1 PLA spots increase, while Dnm2-EndoA1 PLA spots marginally decrease when autophagy is induced. (c) A larger fraction of Dnm2-EndoB1 PLA spots colocalize with LC3 and to a lesser extent with UVRAG when autophagy is induced with rapamycin or CCCP, suggesting that Dnm2 is connected with

autophagy. The fraction that colocalizes with Lamp1 decreases and remains low for Rab11. (d) Overexpressed GFP-Dnm2 spontaneously colocalizes with RFP-LC3 in Dnm2 -/- cells, but not in WT cells. This colocalization is disrupted by the PIKfyve inhibitor YM201636. Enlarged portions of the cells (2X) are shown below each image with merged, Dnm2 (green) and LC3 (red) channels. (e) Colocalization of GFP fused to the PH domain of PLC delta with RFP-LC3 is also observed in Dnm2 -/- cells. (f) Histograms show increased colocalization of the GFP-tagged PH domain of PLC delta with RFP-LC3 in Dnm2 -/- cells. For the histograms, 50 cells per experiment, n=3, unpaired Student's t-test. Scale bar is 10 μm.

Fig. 6. Effects of Dnm2 on Atg9 retrieval from phagophores. (a) RFP-Atg9 colocalizes with EGFP-LC3 in Dnm2 -/- cells treated with CCCP, but not in wild type cells. Similar effects are observed in cells treated with dynasore. (b) Histogram showing increased colocalization of RFP-ATG9 and GFP-LC3 in Dnm2 -/- and dynasore-treated cells after incubation with rapamycin or CCCP. (c) The number of Atg9 vesicles (RFP spots without GFP label) decreases when Dnm2 -/- and dynasore-treated cells are incubated with rapamycin or CCCP. (d, e) Colocalization of VAMP7 with LC3 is increased in Dnm2 -/- cells and increases more after CCCP treatment. (f, g) Colocalization of Fip200 with LC3 is increased in Dnm2 -/- cells and increases more after CCCP treatment. (h, i) There is also increased colocalization of RFP-Atg9 and GFP-LAMP1 after treatment with CCCP. Cells were incubated with pepstatin and E64d to prevent Atg9 digestion in lysosomes. For panels b, c, e, g and i, 50 cells were counted per experiment, n= 3, unpaired students' t-test. (j) Quantification of Atg9 protein levels in wildtype and Dnm2 -/- cells. Levels decrease in Dnm2 -/- cells after treatment with CCCP, but this decrease is partially prevented by Bafilomycin A, suggesting that Atg9 is degraded by autophagy in Dnm2 -/- cells. Band intensities were determined with Licor software, n = 4, unpaired Students' t-test. (k) Models showing EndoB1 in the Vps34 complex and Dnm2 contributing to Atg9 retrieval, most likely as part of a kiss-and-run mechanism for membrane delivery to the phagophore. When Dnm2 is absent, Atg9 mixes with LC3 in phagophores and eventually in autophagosomes. Scale bar is 10 μm for whole cells and 5 μm for enlarged portions.

Suppl. Fig. 1-1 Colocalization of Dnm2 and EndoB1 shown with scatterplots. (a) Scatterplots of immunofluorescence images of cells treated for 2h with or without rapamycin to induce autophagy. (b) Fraction of spots in the colocalizing quadrants of the scatterplots, shown before and after 2 or 4 hr treatment with rapamycin or CCCP. (SD and unpaired Student's t-test, n= 3). (c, d) As in panels a and b, but with transiently expressed GFP- and RFP-tagged proteins.

Suppl. Fig. 1-2. Western blots showing derivation of Dnm2, EndoB1 and DKO cells. Dnm2 and EndoB1 -/- cells were generated by CRISPR/Cas9 in MEFs. DKO cells were generated by additional knockout of EndoB1 in Dnm2 -/- cells. Clone A4 was chosen for further studies.

Suppl. Fig. 1-3. Controls for PLA experiments. (a) PLA signals for Dnm2 and EndoB1 interactions were absent from cells with mutations in one or both of these proteins. (b) As negative control for PLA, cells were incubated with Fis1 and Hsp60 antibodies, which detect proteins that are on the outside or inside of mitochondria and are therefore too far apart for generating PLA signals. As positive control, cells were incubated with antibodies for Drp1 and Mff, which detect well-characterized binding partners. Scale bar is 10 μm.

Suppl. Fig. 2-1. Western blots of Drp1 deletion mutants and Dnm2 conditional knockout cells. (a) Drp1 deletions mutants were generated with CRISPR/Cas9 technology. Clone number 5 was selected for this analysis. (b) Cre-recombinase was induced with tamoxifen at the indicated concentrations for 24 hr and cells were grown for an additional 4 days with fresh medium before western blot analysis of Dnm1 and Dnm2 expression. Although Dnm1 is not normally expressed in these cells and Dnm3 is undetectable with currently available antibodies (Park et al. 2013), all three genes were floxed with 3 μM tamoxifen to ensure complete lack of dynamins.

Suppl. Fig. 2-2. Effects of Dnm2 and EndoB1 mutations on mitochondrial fission shown with live cells. The images show MEFs transfected with mitochondrial DsRed and genotypes as indicated. Cells were treated with or without 20 μM CCCP for 30min. Scale bar is 10 μm.

Suppl. Fig. 4-1. Western blots showing accumulation of optineurin in Dnm2 -/- cells. Optineurin is degraded when mitophagy is induced, but this degradation is not prevented by Bafilomycin A, suggesting that it can be degraded by other mechanisms. Optineurin accumulation could nevertheless, still accelerate mitophagy in Dnm2 -/- cells.

Suppl. Fig. 6-1. Effects of Dnm2 siRNA on Atg9 retrieval. (a) Western blot showing depletion of Dnm2 after transfection with siRNA oligonucleotides. (b) RFP-Atg9 colocalizes with EGFP-LC3 after treatment with CCCP in Dnm2 siRNA cells, but not in mock-transfected cells. (c) Histogram showing increased colocalization of RFP-ATG9 and GFP-LC3 in CCCP-treated Dnm2 siRNA cells. Scale bar is 10 μm for whole cells and 5 μm for enlarged portions.

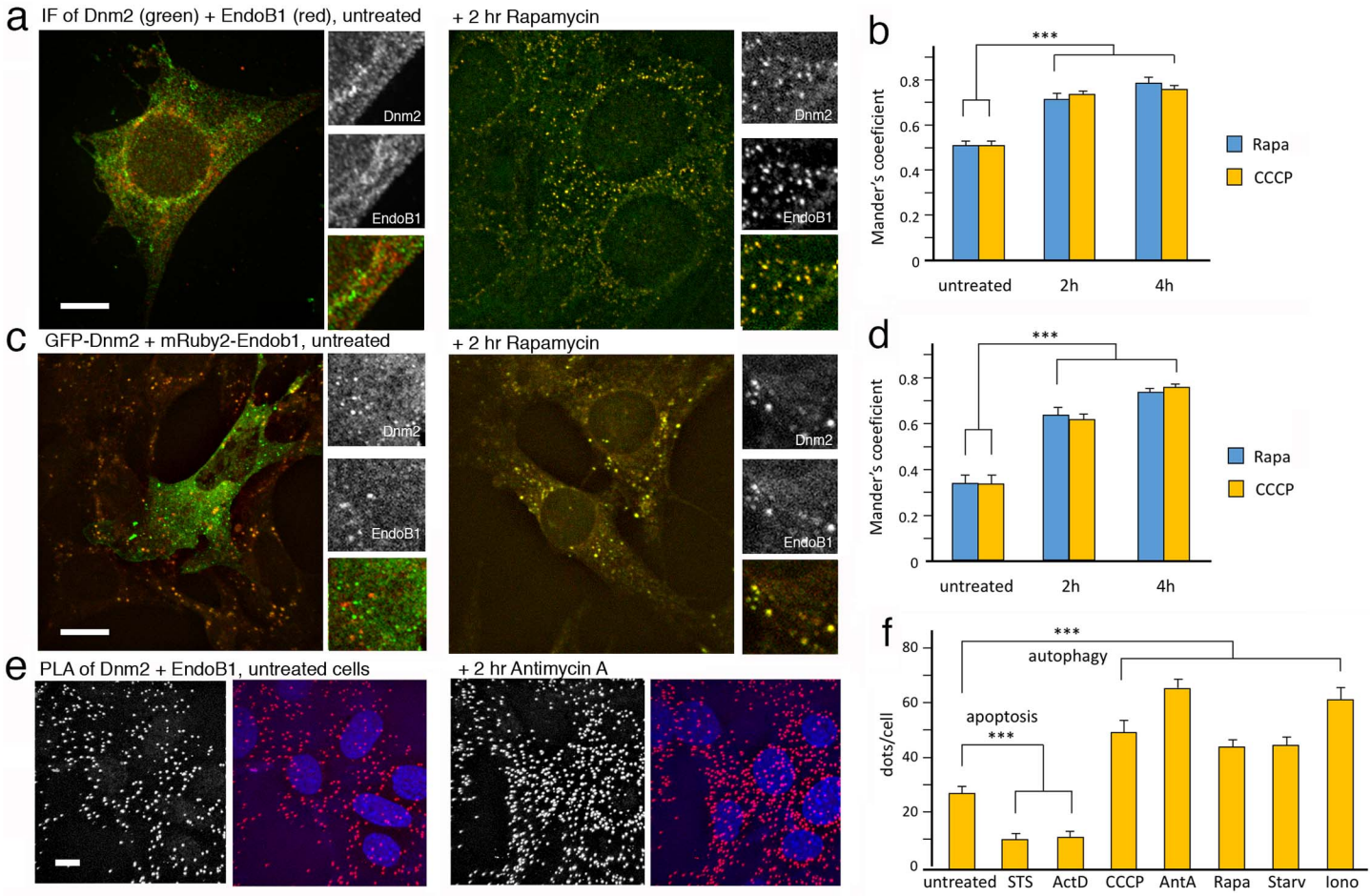
a
IF of Dnm2 (green) + EndoB1 (red), untreated
+ 2 hr Rapamycin
Dnm2
EndoB1
b
***
Mander's coeeficient
0
0.2
0.4
0.6
0.8
untreated
2h
4h
Rapa
CCCP
c
GFP-Dnm2 + mRuby2-Endob1, untreated
+ 2 hr Rapamycin
Dnm2
EndoB1
d
***
Mander's coeeficient
0
0.2
0.4
0.6
0.8
untreated
2h
4h
Rapa
CCCP
e
PLA of Dnm2 + EndoB1, untreated cells
+ 2 hr Antimycin A
f
***
autophagy
apoptosis
***
dots/cell
0
20
40
60
80
untreated
STS
ActD
CCCP
AntA
Rapa
Starv
Iono

Figure 1

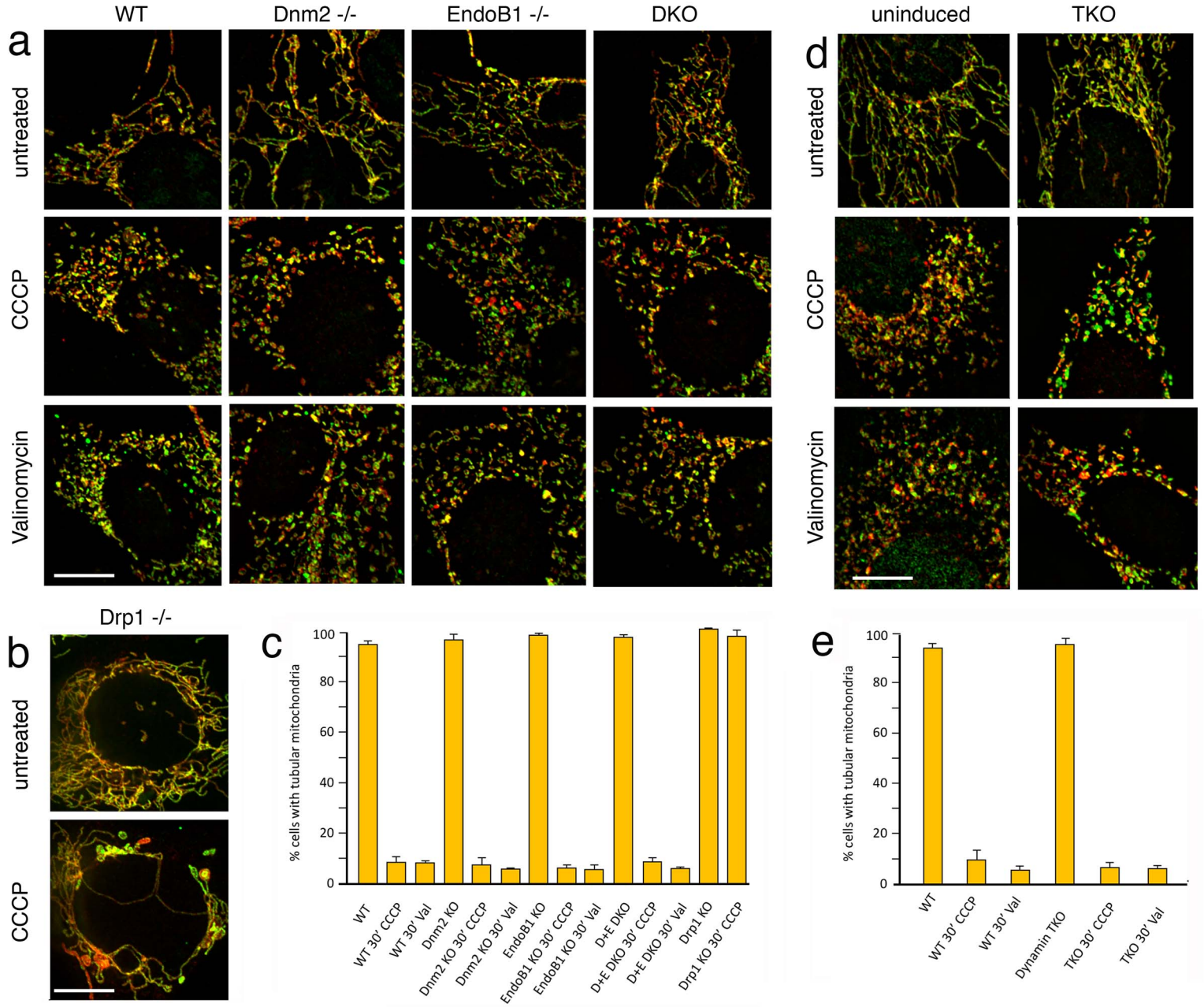
a
WT
Dnm2 -/-
EndoB1 -/-
DKO
untreated
CCCP
Valinomycin
d
uninduced
TKO
untreated
CCCP
Valinomycin
b
Drp1 -/-
untreated
CCCP
c
% cells with tubular mitochondria
0
20
40
60
80
100
WT
WT 30' CCCP
WT 30' Val
Dnm2 KO
Dnm2 KO 30' CCCP
Dnm2 KO 30' Val
EndoB1 KO
EndoB1 KO 30' CCCP
EndoB1 KO 30' Val
D+E DKO
D+E DKO 30' CCCP
D+E DKO 30' Val
Drp1 KO
Drp1 KO 30' CCCP
e
% cells with tubular mitochondria
0
20
40
60
80
100
WT
WT 30' CCCP
WT 30' Val
Dynamin TKO
TKO 30' CCCP
TKO 30' Val

Figure 2

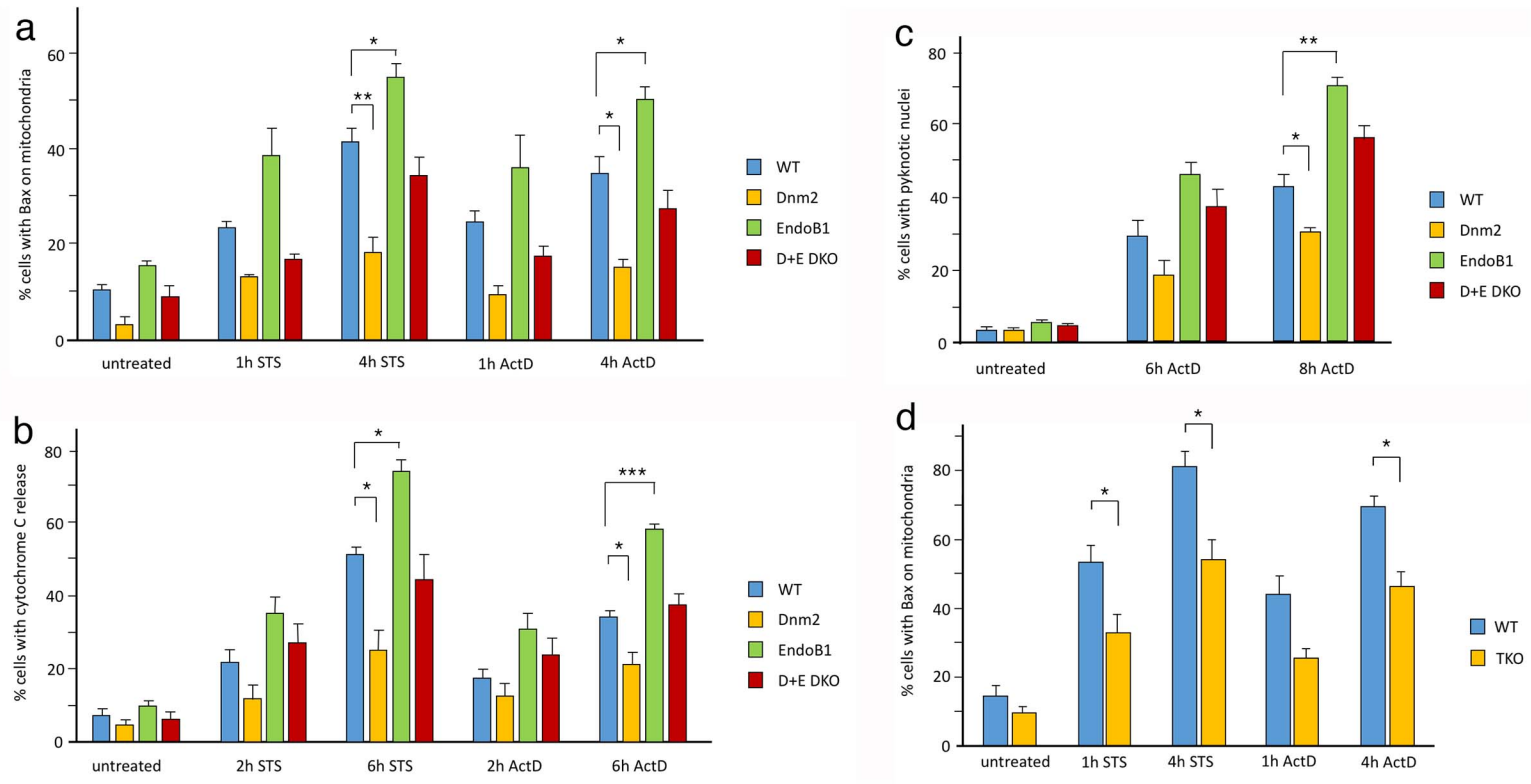
a
% cells with Bax on mitochondria
0
20
40
60
untreated
1h STS
4h STS
1h ActD
4h ActD
*
**
*
*
WT
Dnm2
EndoB1
D+E DKO
b
% cells with cytochrome C release
0
20
40
60
80
untreated
2h STS
6h STS
2h ActD
6h ActD
*
*
***
*
WT
Dnm2
EndoB1
D+E DKO
c
% cells with pyknotic nuclei
0
20
40
60
80
untreated
6h ActD
8h ActD
**
*
WT
Dnm2
EndoB1
D+E DKO
d
% cells with Bax on mitochondria
0
20
40
60
80
untreated
1h STS
4h STS
1h ActD
4h ActD
*
*
*
WT
TKO

Figure 3

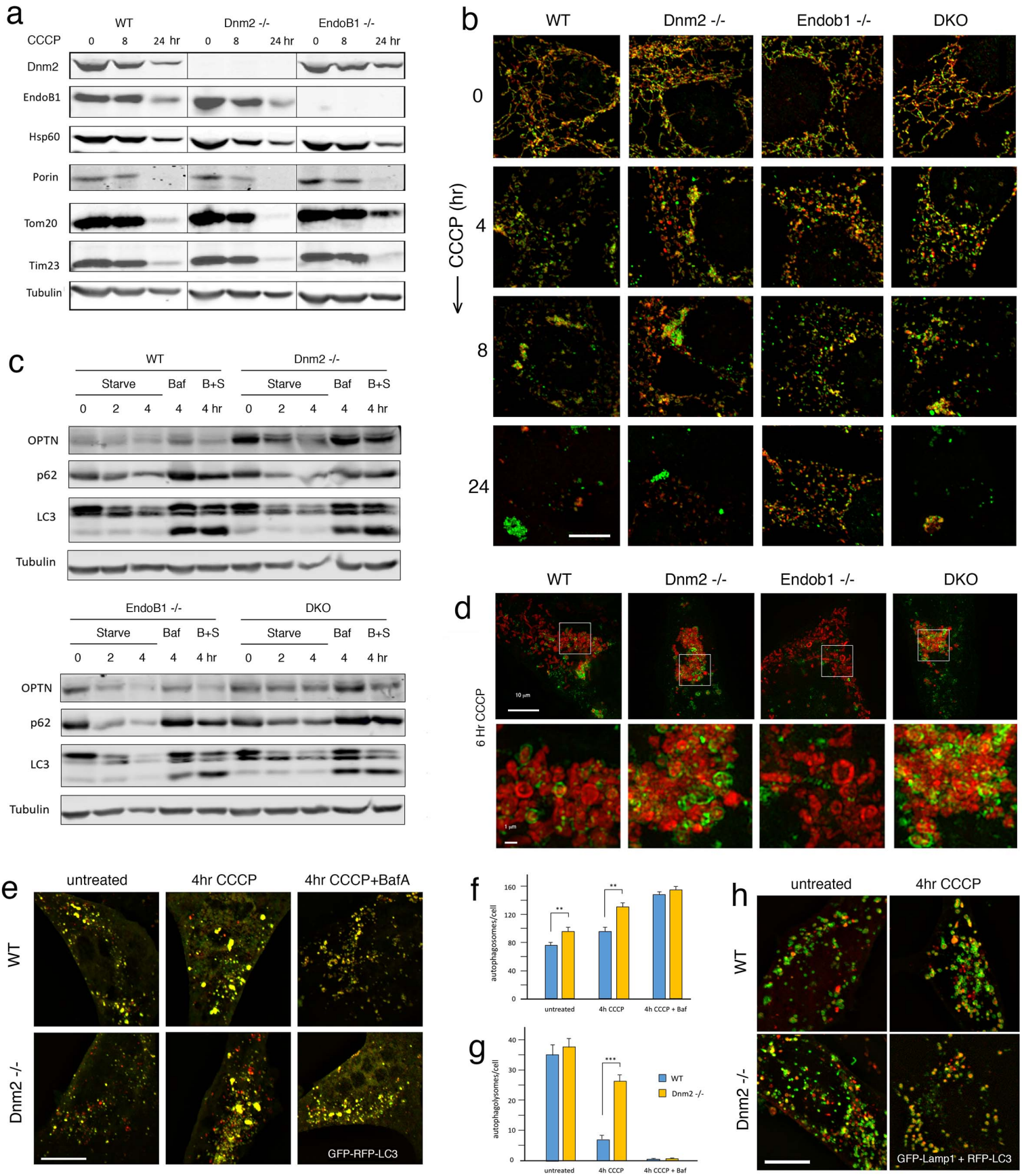
a
WT
Dnm2 -/-
EndoB1 -/-
CCCP
0
8
24 hr
Dnm2
EndoB1
Hsp60
Porin
Tom20
Tim23
Tubulin
b
WT
Dnm2 -/-
Endob1 -/-
DKO
CCCP (hr)
0
4
8
24
c
WT
Dnm2 -/-
Starve
Baf
B+S
0
2
4
4
4 hr
OPTN
p62
LC3
Tubulin
EndoB1 -/-
DKO
d
6 Hr CCCP
10 µm
1 µm
e
untreated
4hr CCCP
4hr CCCP+BafA
GFP-RFP-LC3
f
autophagosomes/cell
untreated
4h CCCP
4h CCCP + Baf
g
autophagolysomes/cell
WT
Dnm2 -/-
h
GFP-Lamp1 + RFP-LC3

Figure 4

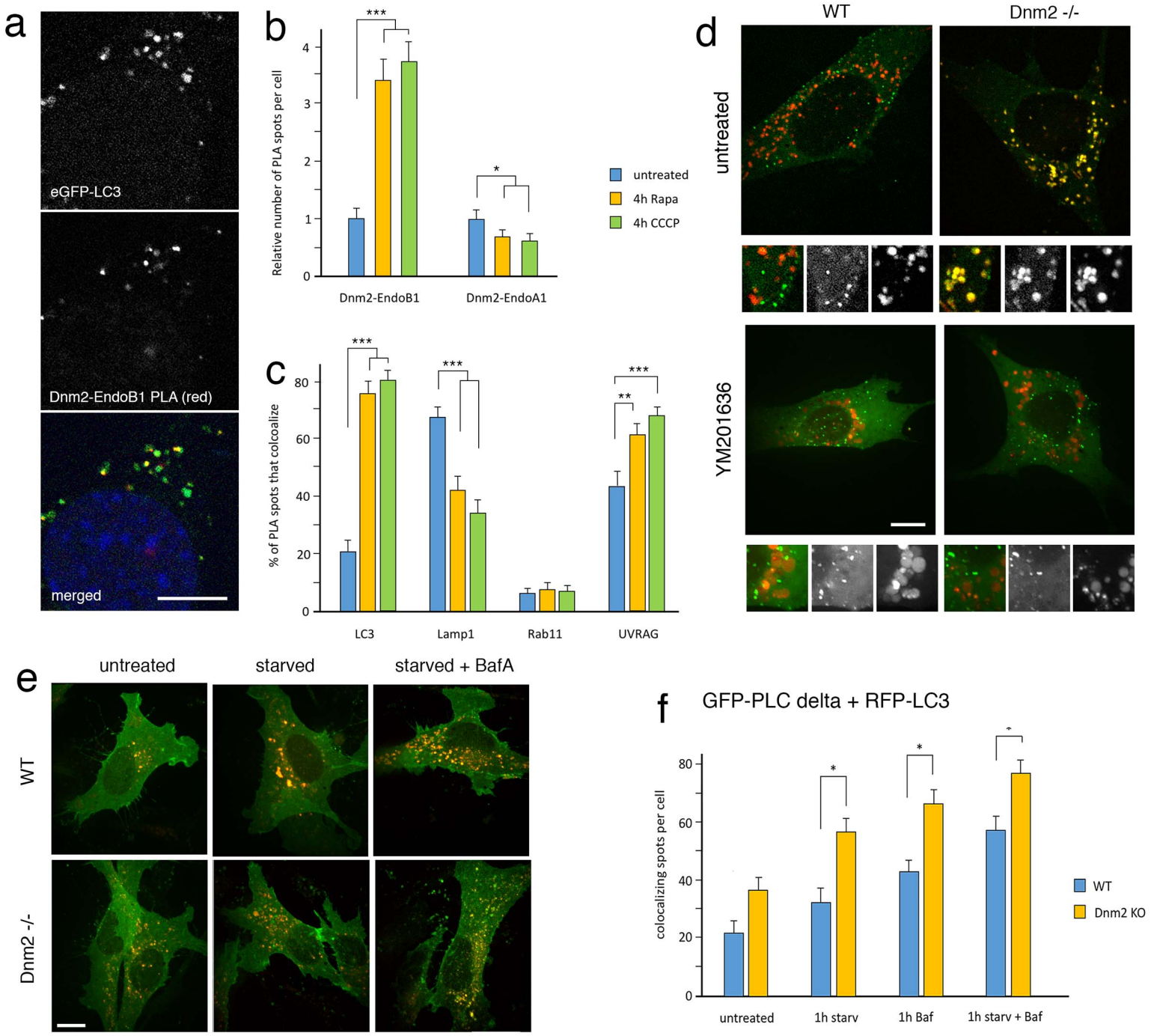
a
eGFP-LC3
Dnm2-EndoB1 PLA (red)
merged
b
Relative number of PLA spots per cell
Dnm2-EndoB1
Dnm2-EndoA1
untreated
4h Rapa
4h CCCP
c
% of PLA spots that colcoalize
LC3
Lamp1
Rab11
UVRAG
d
WT
Dnm2 -/-
untreated
YM201636
e
untreated
starved
starved + BafA
WT
Dnm2 -/-
f
GFP-PLC delta + RFP-LC3
colocalizing spots per cell
untreated
1h starv
1h Baf
1h starv + Baf
WT
Dnm2 KO

Figure 5

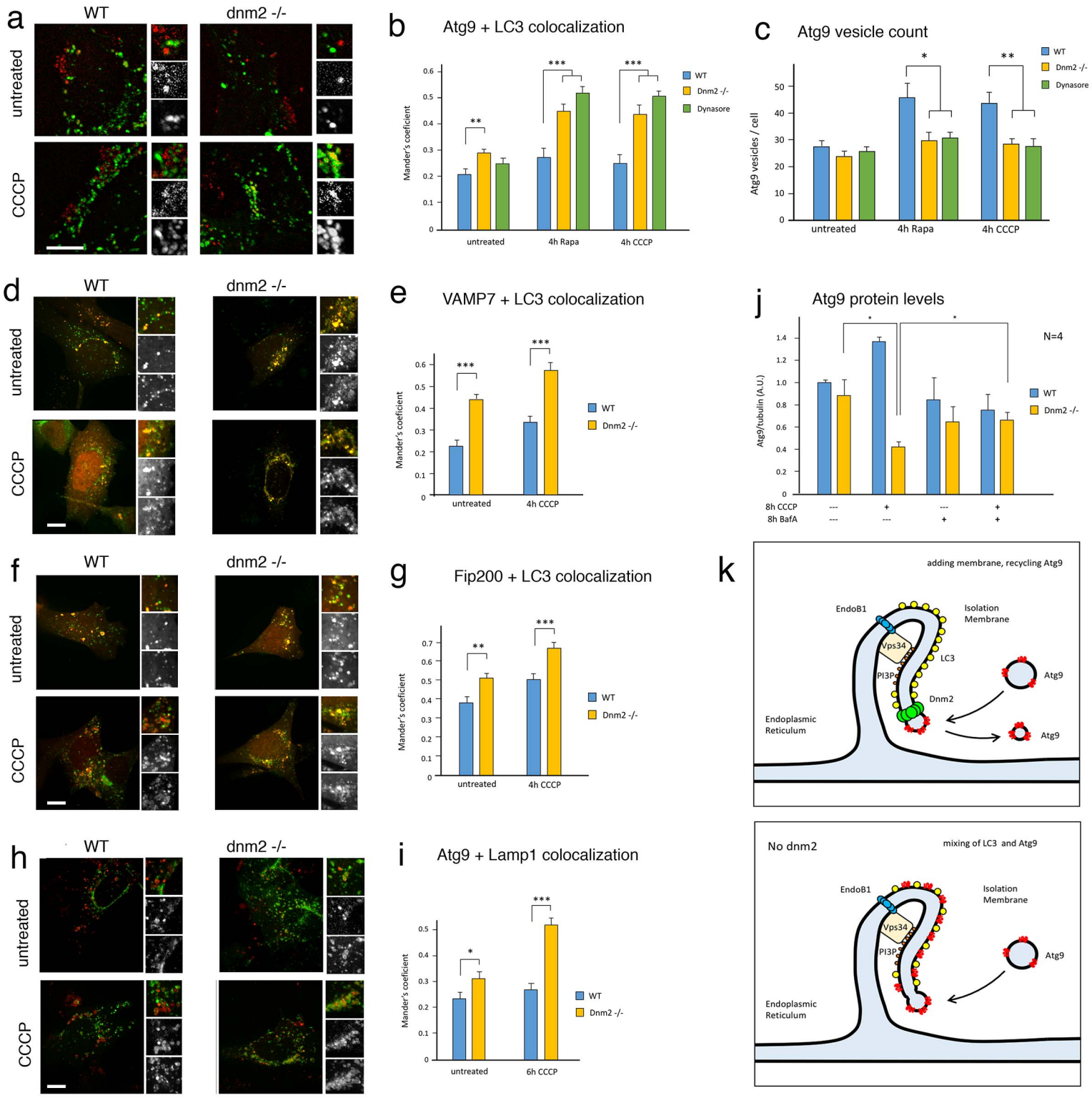
a
WT
dnm2 -/-
untreated
CCCP
b
Atg9 + LC3 colocalization
Mander's coeficient
WT
Dnm2 -/-
Dynasore
untreated
4h Rapa
4h CCCP
c
Atg9 vesicle count
Atg9 vesicles / cell
d
e
VAMP7 + LC3 colocalization
j
Atg9 protein levels
Atg9/tubulin (A.U.)
N=4
8h CCCP
8h BafA
f
g
Fip200 + LC3 colocalization
k
adding membrane, recycling Atg9
EndoB1
Isolation Membrane
Vps34
LC3
PI3P
Dnm2
Atg9
Endoplasmic Reticulum
h
i
Atg9 + Lamp1 colocalization
6h CCCP
No dnm2
mixing of LC3 and Atg9

Figure 6

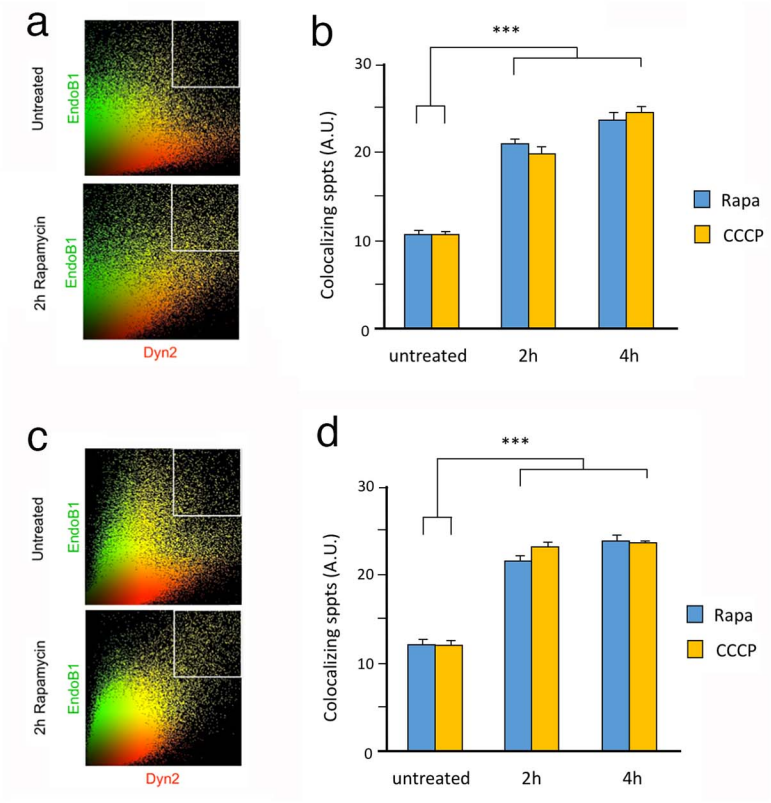
a
Untreated
EndoB1
2h Rapamycin
EndoB1
Dyn2
b
***
Colocalizing sppts (A.U.)
30
20
10
0
untreated
2h
4h
Rapa
CCCP
c
Untreated
EndoB1
2h Rapamycin
EndoB1
Dyn2
d
***
Colocalizing sppts (A.U.)
30
20
10
0
untreated
2h
4h
Rapa
CCCP

Suppl. Fig. 1-1

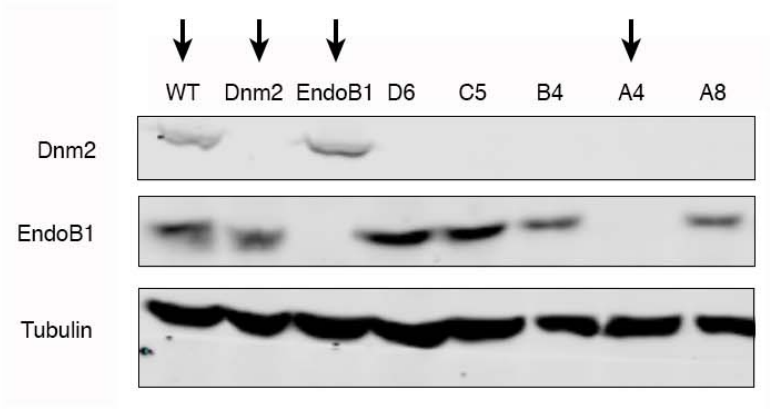

Suppl. Fig. 1-2

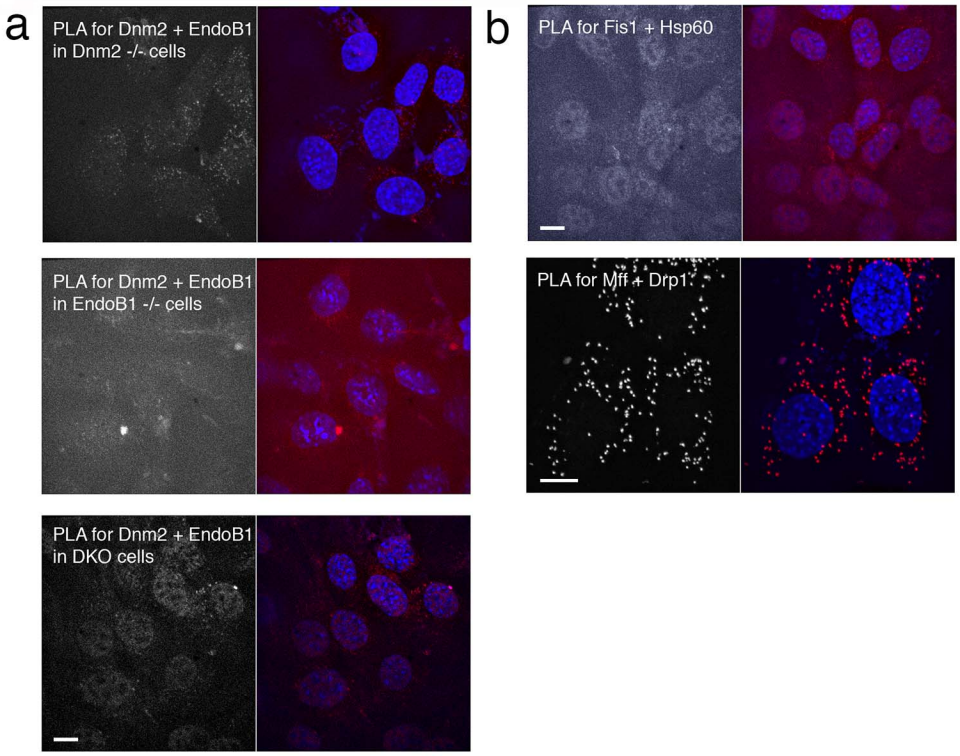
a
PLA for Dnm2 + EndoB1
in Dnm2 -/- cells
PLA for Dnm2 + EndoB1
in EndoB1 -/- cells
PLA for Dnm2 + EndoB1
in DKO cells
b
PLA for Fis1 + Hsp60
PLA for Mff + Drp1

Suppl. Fig. 1-3

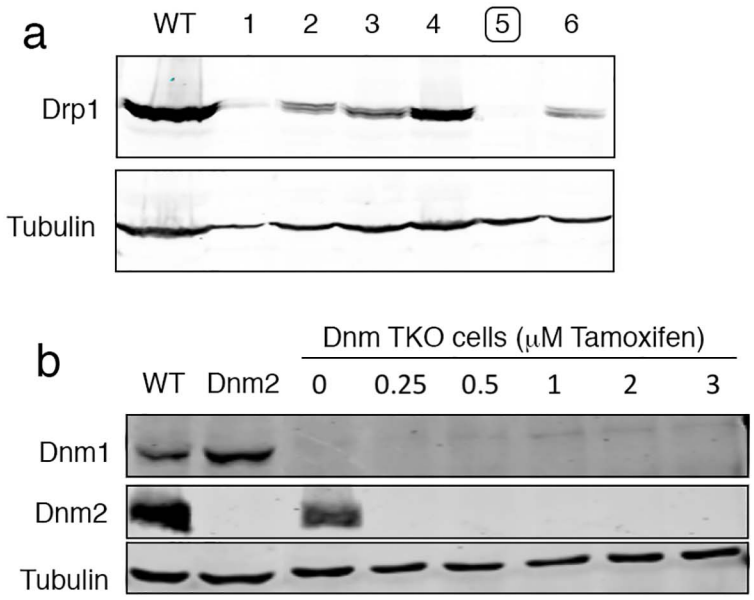
a
WT
1
2
3
4
5
6
Drp1
Tubulin
b
Dnm TKO cells (μM Tamoxifen)
WT
Dnm2
0
0.25
0.5
1
2
3
Dnm1
Dnm2
Tubulin

Suppl. Fig. 2-1

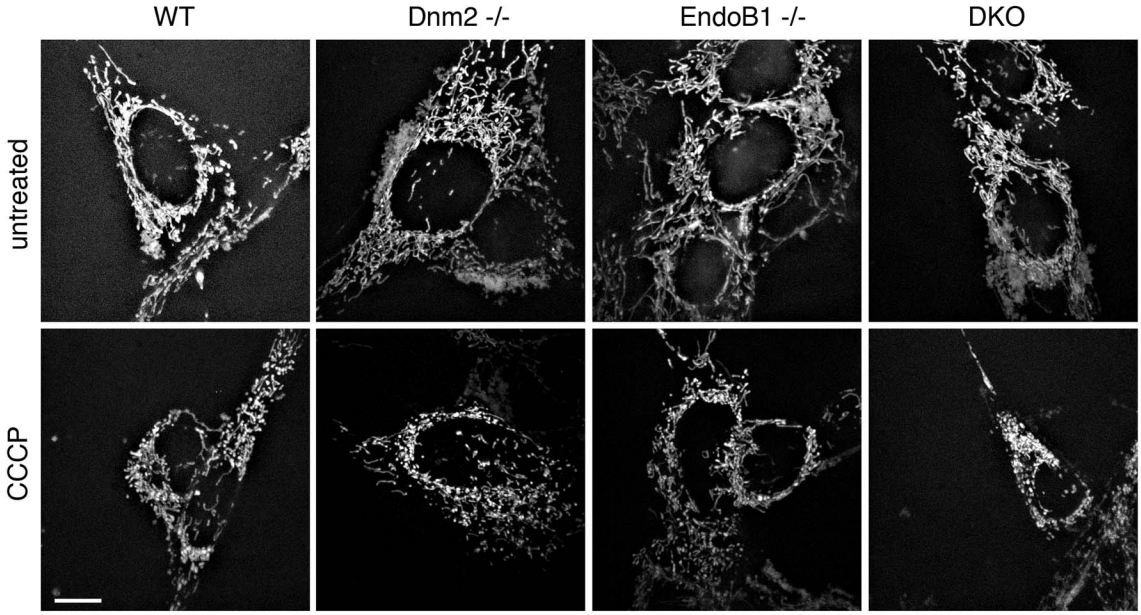

Suppl. Fig. 2-2

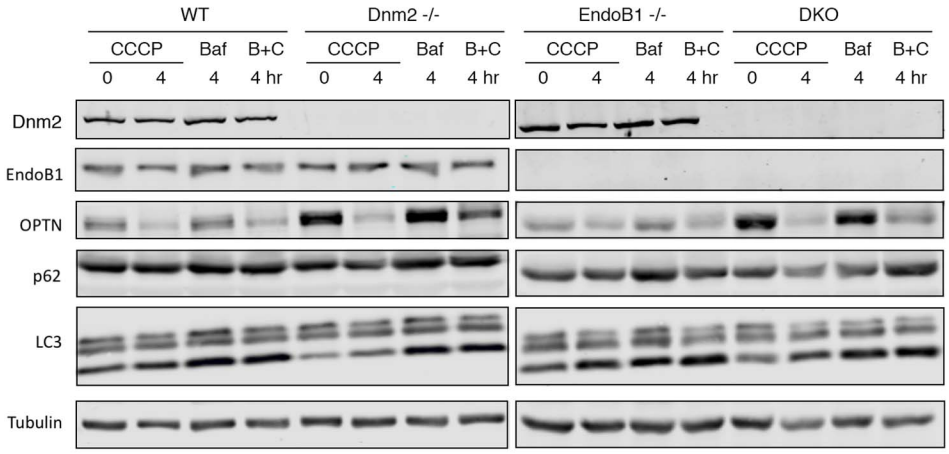
WT
Dnm2 -/-
EndoB1 -/-
DKO
CCCP
Baf
B+C
0
4
4
4 hr
Dnm2
EndoB1
OPTN
p62
LC3
Tubulin

Suppl. Fig. 4-1

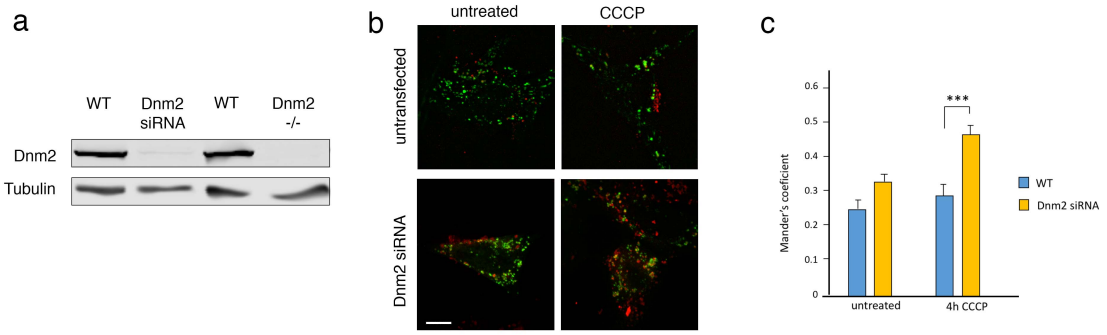
a
WT
Dnm2 siRNA
WT
Dnm2 -/-
Dnm2
Tubulin
b
untreated
CCCP
untransfected
Dnm2 siRNA
c
Mander's coeficient
0.6
0.5
0.4
0.3
0.2
0.1
0
***
untreated
4h CCCP
WT
Dnm2 siRNA

Suppl. Fig. 6-1